Progress In Electromagnetics Research B, Vol. 60, 141–155, 2014

Overview of Ionospheric Modification by High Frequency (HF) Heaters-Theory

Spencer P. Kuo*

Abstract—The scenarios of achieving effective ionospheric modification are summarized and the likely physical processes engaging linear and nonlinear mode conversions through plasma inhomogeneity and nonlinearity are revealed. Parametric instabilities, which are the directly relevant processes to achieve effective heating of the ionospheric F region, are formulated and analyzed. The threshold fields and growth rates of instabilities are obtained. The nonlinear Schrodinger equation governing the nonlinear evolution of Langmuir waves is derived and analyzed. The nonlinear periodic and solitary solutions of the equation are obtained. The analyses illustrate the conditions for the generation of Langmuir soliton and nonlinear periodic Langmuir waves.

1. INTRODUCTION

Observations of ionospheric HF heating experiments in the past four decades have demonstrated that the HF heater can significantly modify the bottomside of the ionospheric F-region. It occurs when the HF transmitter is operated with frequency less than f_oF2 and the HF heater is transmitted at RH circular polarization so that it is converted to the O-mode in the region near the HF reflection height. Because the collision (electron-electron and electron-ion) processes cannot efficiently absorb the electromagnetic (EM) wave energy delivered to the F region of the ionosphere, these requirements on the transmitted HF heater in the experiments are necessary in order to effectively trap the wave energy there and thus to optimize the HF modification effects on the ionosphere. However, the HF heater can be reflected back to the ground. To avoid this to occur, a fast conversion of the EM heating wave into electrostatic (ES) waves of the plasma is necessary. This is because ES waves are supported by the plasma and only stay in the plasma. Thus, linear and nonlinear mode conversions are essential processes acting to achieve effective ionospheric heating and modification [1].

The present work is aimed at providing theoretical foundation for the understanding of experimental observations and the underlying plasma processes. The responsible physical processes of the observations evidence that the excitation of parametric instabilities is essential to all observations.

2. MODE CONVERSION

An EM wave can be converted into ES waves in plasma through linear or nonlinear mode conversion. Before a discussion on mode conversion, a comment on the mode types is in order. In general, wave is characterized by its frequency and wavelength. In plasma, wave is also characterized by the direction of the wave electric field (i.e., the polarization direction) with respect to the wave propagation direction, which divides the plasma waves into three categories representing three mode types: transverse (EM), longitudinal (ES), and hybrid. Transverse means that the wave electric field is transverse (perpendicular) to the wave propagation direction; hence, transverse wave is an EM wave that also carries a magnetic

Received 18 April 2014, Accepted 18 June 2014, Scheduled 25 June 2014

* Corresponding author: Spencer P. Kuo (skuo@poly.edu).
The author is with the Department of Electrical & Computer Engineering, Polytechnic School of Engineering, New York University, 5 MetroTech Center, Brooklyn, NY 11201, USA.

field. Longitudinal means that the wave electric field is parallel to the propagation direction; in essence, it is an ES wave because no magnetic field accompanies the wave electric field. Plasma is anisotropic when a dc magnetic field is imposed; the wave electric field may have an angle other than 0° or 90° with respect to the propagation direction (i.e., a combination of EM and ES polarization). In this situation, the wave is a hybrid mode.

A mode of a linear system is an oscillation that can self-sustain in the system. For example, apply an impulse to a (lossless) system; oscillations at all frequencies will be excited. However, not all of the oscillations can persist in time; in fact, most of the oscillations will damp away via phase mixing (among themselves or caused by the boundary effects). In the steady state, only a few oscillations remain, and these lasting oscillations are the "modes" of the system. In a lossless system, modes are not damped and termed "eigen-modes". In practice, system has losses and supports only "quasi-modes", which damp slowly in time. In the mathematical analysis, modes represent the source-free space-time harmonic solutions of the system's linearized governing equations. Therefore, (ω-k) relations are determined by the condition that the space-time harmonic solutions of the source-free equations are nontrivial (i.e., nonzero solutions). Each relation $\omega = \omega(k)$ is called a dispersion relation, which can be plotted on a k-ω plane as the dispersion curve of a branch of mode. Each point (k, ω) on the curve defines the wavenumber and frequency of a mode in that branch.

Linear mode conversion may occur in the ionosphere because it is inhomogeneous magneto plasma. Magneto plasma supports various branches of plasma modes, which are EM, ES, or hybrid mode type depending on the frequency regime, the polarization direction, and the propagation angle with respective to the geomagnetic field. As explained in the preceding paragraph, a dispersion relation represents a branch of plasma mode and is a functional dependence of the wave frequency ω on the propagation constant k. Magneto plasma is an anisotropic (uniaxial) medium, ω is a function of $k_{||}$ and $k_{\perp}$, where the subscripts $||$ and $\perp$ stand for components parallel and perpendicular to the magnetic field; the dispersion curves $\omega\,(k_{||}, k_{\perp})$ of magneto plasma are presented in three-dimensional spectral space ($k_{||}$, $k_{\perp}$, ω). However, a conventional way, which makes easy to describe the physical processes of wave propagation in inhomogeneous magneto plasma, is to plot the dispersion curves of the 0° and 90° propagation angles only; in these special cases, ω are functions of $|\mathbf{k}|\,(= k)$. Thus these curves can be combined together in a single two-dimensional diagram on the k-ω plane, such as the one exemplified in Fig. 1(a) (upward propagating waves in cold plasma embedded in a downward magnetic field). In this figure, only high frequency branches relevant to the following discussion are plotted and the cutoff frequencies ω_1 [for the left-hand (LH) circularly polarized (L) and extraordinary (X) branches] and ω_2 [for the right-hand (RH) circularly polarized (R) branch] and upper hybrid resonance frequency ω_u are given. Hence, a branch for an arbitrary propagation angle can be located in the region between a pair of 0° and 90° branches.

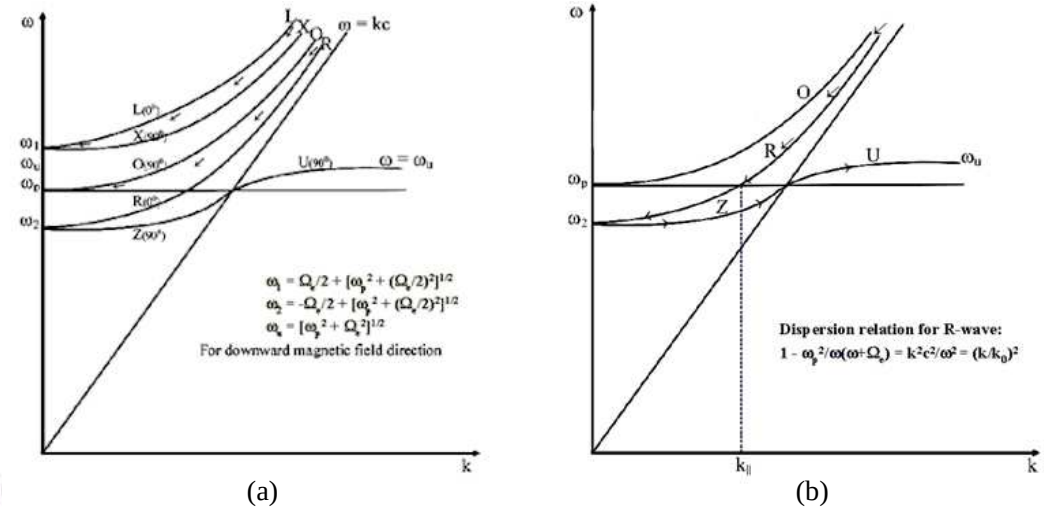

Figure 1. (a) Dispersion curves of high frequency EM waves propagating along (0°) and perpendicular (90°) to the geomagnetic field and (b) dispersion curves for a RH circularly polarized incident wave.

Among the curves in Fig. 1(a), L and X is a pair to confine the X-mode branches having the propagation angle between 0° and 90° because in the case of propagating anti-parallel to the magnetic field, the wave fields of the L mode rotate in the same direction as the electron gyration. Likewise, R and O pair confine the ordinary (O-mode) branches. The polarization of the incident heating wave determines the branch of mode it belongs to. Left-hand (LH) circularly polarized heater falls into the X-mode branches, and right-hand (RH) circularly polarized heater follows the O-mode branches in the propagation. It is noted that Fig. 1(a) is plotted for uniform plasma, i.e., in the case of constant plasma frequency ω_p and electron cyclotron frequency Ω_e. However, the ionosphere is not uniform; although Ω_e may be considered to be a constant at each heating site, ω_p increases with the altitude in the bottom-side of the ionosphere. As a HF heater of a fixed frequency ω_0 propagates upward, ω_p in Fig. 1(a) moves upward along the vertical (ω) axis. Consequently, all the dispersion curves will also move upward accordingly. This will be inconvenient in describing wave propagation because Fig. 1(a) has to be modified constantly. However, there is a way to fix ω_p on the vertical axis of Fig. 1(a); it is by constantly rescaling the ω axis during the wave propagation. For example, as wave propagates upward, the scale of the ω axis is increased accordingly to keep ω_p at the same point on the axis. Consequently, the initial point (k_0, ω_0) of the wave has to move downward, but confined in the region between a pair of 0° and 90° branches. The arrows in Fig. 1(a) indicate the trajectories, in the k-ω plane, of vertically incident LH (X-mode) and RH (O-mode) circularly polarized waves. The two incident waves start with the same propagation angle equal to the conjugate α of the magnetic dip angle θ_d, where θ_d is defined to be the angle between the horizontal axis and the geomagnetic field that is inclined downward in the northern hemisphere. As shown the point of LH circularly polarized incident wave moves downward and its trajectory gradually merges to the $L\,(0^\circ)$ curve; the wave is reflected at $\omega_p = [\omega_0(\omega_0 - \Omega_e)]^{1/2} = \omega_{pL}$. On the other hand, the trajectory of the point representing the RH circularly polarized incident wave gradually merges to the $O\,(90^\circ)$ curve and the wave is reflected at $\omega_p = \omega_0$, higher than the reflection height of the LH circularly polarized incident wave.

2.1. Linear Mode Conversion

Linear mode conversion may occur at the intersecting point of two branches of modes. As shown in Fig. 1(a) only the O-mode branch intersects with the branches of plasma modes. Thus the HF heater has to be transmitted at RH circular polarization and Fig. 1(b) will be used in the discussion of linear mode conversion. In the figure, only the dispersion curves of the R and O pair are plotted and $k_{||}$ in the plot represents the parallel (to the geomagnetic field) component of the wavevector.

The arrows in Fig. 1(b) signify the transmission of a RH circularly polarized HF heater, with an oblique incident angle θ_0, into the ionosphere; the vertical component of the wavevector, with the initial value $k_0 \cos\theta_0$, decreases continuously as the heater propagates upward to experience the increase of the plasma density, where $k_0 = \omega_0/c$ and ω_0 is the wave frequency. Consequently, the inclined angle of the propagation, with respective to the geomagnetic field, also changes continuously. When the wave approaches the O-mode reflection height indicated by the horizontal line $\omega = \omega_p$, the propagation turns toward either 1) the O-curve or 2) the R-curve, depending on the initial inclined angle (related to the incident angle). In either cases, the wave will reach an intersecting point on the $\omega = \omega_p$ line. In the first situation, for example, for a vertically incident wave ($\theta_0 = 0$), the propagation turns toward the direction perpendicular to the geomagnetic field (with the wavevector $\mathbf{k} \to 0$). The intersecting point located at ($k = 0$, $\omega_0 = \omega_p$) is a turning point (cutoff), where the wave is reflected. Because the propagation direction of the wave in the nearby region is drastically different from that of the electron plasma wave (i.e., Langmuir wave), which has a preferred propagation direction parallel to the geomagnetic field; therefore, a mode conversion of the heater to the Langmuir wave is not feasible.

The second situation that the propagation turns to follow the R-curve as shown by the arrows requires a proper incident angle of the heater. In this case, the wave at the intersecting point ($k = k_{||}$, $\omega_0 = \omega_p$) does not experience cutoff from propagation. Because the ionospheric plasma density is horizontally stratified, the horizontal component, $k_0 \sin\theta_s$ in Fig. 2, of the initial wave vector $\mathbf{k}_0$ is conserved in the propagation. Thus the horizontal component, $k_{||} \sin\alpha$ in Fig. 2, of the wavevector $\mathbf{k}_{||}$ at the intersecting point equals to $k_0 \sin\theta_s$, i.e., $k_0 \sin\theta_s = k_{||} \sin\alpha$. If the wave propagates continuously upward along the geomagnetic field, then ($k_{||}$, ω_0) have to satisfy the R-wave dispersion relation:

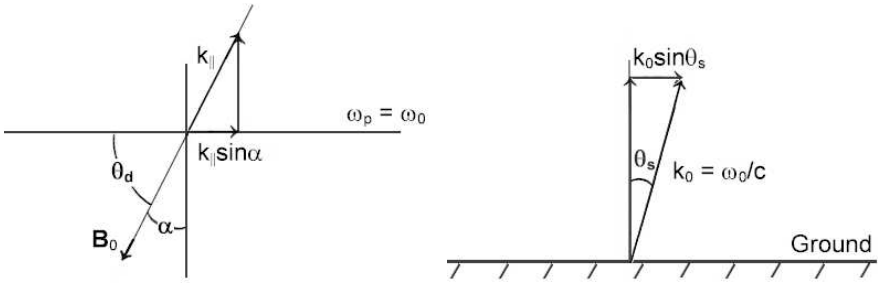

Figure 2. Phase matching condition for mode conversion.

$1 - \omega_p^2/\omega(\omega + \Omega_e) = (kc/\omega)^2$, under the condition $\omega_0 = \omega_p$.

Therefore the required incident (Spitze) angle is derived by the phase matching condition $k_0 \sin\theta_s = k_{||} \sin\alpha$, subject to that ($k_{||}$, $\omega_0 = \omega_p$) satisfy the R-wave dispersion relation. From the dispersion relation, we obtain $k_{||} = k_0[\Omega_e/(\omega_0 + \Omega_e)]^{1/2}$, and the Spitze angle is determined to be

$$\theta_s = \sin^{-1}\left\{[\Omega_e/\left(\omega_0 + \Omega_e\right)]^{1/2} \sin\alpha\right\} \tag{1}$$

After passing the $\omega_p = \omega_0$ layer, wave continuously propagates upward along the geomagnetic field to a cutoff layer at $\omega_p = [\omega_0(\omega_0 + \Omega_e)]^{1/2} = \omega_{pR}$, where the wave is reflected at an oblique angle of 2α and converted to a Z-mode in the region above the O-mode reflection height. This Z-mode wave propagates downward to the upper hybrid resonance layer at $\omega_p = (\omega_0^2 - \Omega_e^2)^{1/2} = \omega_{pU}$ and is converted to an upper hybrid wave.

Through this linear mode conversion [2], the O-mode HF heater wave energy will be trapped in the region between $\omega_p = \omega_{pR}$ and ω_{pU} layers.

2.2. Nonlinear Mode Conversion

Another effective way (and probably the most effective way) to convert the HF heater to the plasma waves is through parametric instabilities, which excite high frequency electron waves and low frequency ion waves simultaneously by the HF heater. This is a nonlinear mode conversion process employing the nonlinearity of plasma to implement mode-mode couplings and to channel feedbacks to the interactions. The couplings are imposed by the frequency and wavevector matching conditions. The process prefers the excited waves (in particular, the high frequency electron waves) to be plasma modes to reduce the threshold condition for the commencement of the instability. Thus the HF heater has to be accessible to the regions where the frequencies of the high frequency plasma modes are close to the heater frequency. As shown in Fig. 1(a), the vertically incident LH circularly polarized HF heater (X-mode) is reflected at a height with $\omega_{pX} = [\omega_0(\omega_0 - \Omega_e)]^{1/2} = \omega_{pL}$ that is below the electron plasma resonance layer $\omega_{pO} = \omega_0$ as well as the upper hybrid resonance layer $\omega_{pU} = (\omega_0^2 - \Omega_e^2)^{1/2}$. On the other hand, the vertically incident RH circularly polarized HF heater (O-mode) is accessible to both the electron plasma layer and upper hybrid resonance layer and converted to the O-mode in the region close to its reflection height. In other words, the O-mode HF heater is accessible to the spatial regions, where many parametric coupling conditions can be matched. Moreover, near the reflection height the O-mode heater's electric field is enhanced by a "swelling effect", which is arisen from the total reflection at cutoff, providing a factor of $\sim$2, and from wave accumulation in slowing down the propagation while approaching the turning point, providing additional factor of $\sim$2. This "swelling effect" has significant positive impact on exciting instabilities in this region. It makes easy to exceed the threshold fields and increases the growth rates of the instabilities.

3. PARAMETRIC INSTABILITIES

A parametric amplifier uses three coupled resonant circuits (e.g., LC circuits) to convert frequency from one to another. A nonlinear (variac) capacitor C in the circuit provides the coupling (i.e., frequency

mixing). The three resonant modes, oscillating at ω_0, ω_1, and ω_S, in a parametric amplifier are called source (pump), idler (sideband), and signal (decay mode), where, the frequency matching condition $\omega_0 = \omega_1 + \omega_S$ is satisfied. Generalize the basic principle for wave amplification in a circuit to a system, one recognizes that the system has to support at least three branches of oscillations and carries nonlinear properties for wave-wave couplings.

Plasma can support high frequency EM waves, as well as electrostatic (ES) plasma waves of high and low frequencies as plasma modes that oscillate in plasma as thermal fluctuations in the absence of external sources. Moreover, plasma is a nonlinear medium. Therefore, parametric couplings among three modes can occur. When a large amplitude high frequency wave $\mathbf{E}_p(\omega_0, \mathbf{k}_p)$ (either EM or ES) appears in plasma, this wave can act as a pump wave to excite plasma modes through parametric couplings. The electric field of the high frequency pump wave sets up a quiver motion $v_{eq}(t)$ in the electron plasma. The quasi-neutrality permits low frequency plasma wave to set up charge density perturbation $n_s(\omega_s, \mathbf{k}_s)$, in which the electrons undergoe quiver motion. Thus a nonlinear current density $-en_s v_{eq}$ is produced. It is a source current to drive beat waves $\mathbf{E}_1(\omega_1, \mathbf{k}_1)$ and $\mathbf{E}_1'(\omega_1', \mathbf{k}_1')$ with their wavevectors and frequencies governed by the matching conditions:

$$\omega_0 = \omega_1 + \omega_s^* = \omega_1' - \omega_s \quad \text{and} \quad \mathbf{k}_p = \mathbf{k}_1 + \mathbf{k}_s = \mathbf{k}_1' - \mathbf{k}_s \tag{2}$$

These beat waves, in turn, also couple with the pump wave to give rise a low frequency nonlinear force on electrons; this force drives a plasma density perturbation which oscillates at the same frequency and wavevector as $n_s(\omega_s, \mathbf{k}_s)$. Hence, this parametric coupling produces a feedback to the original density perturbation $n_s(\omega_s, \mathbf{k}_s)$. The strength of the coupling depends on the involved nonlinearities and the nature of the induced beat waves. The coupling is strong as the beat wave is resonant with plasma (i.e., a plasma mode). If the feedback is positive and large enough to overcome linear losses of the coupled waves, the coupling becomes unstable and coupled waves grow exponentially in the expense of pump wave energy. This is called "parametric instability", by which the pump wave $\mathbf{E}_p(\omega_0, \mathbf{k}_p)$ decays to two sidebands $\mathbf{E}_1(\omega_1, \mathbf{k}_1)$ and $\mathbf{E}_1'(\omega_1', \mathbf{k}_1')$ through a low frequency decay mode $n_s(\omega_s, \mathbf{k}_s)$. This instability process involves the nonlinearity of the plasma and thus is a nonlinear instability. The parametric coupling is imposed by the frequency and wavevector matching conditions (2) as well as a threshold condition on the pump electric field intensity.

This process can be reduced to a three-wave coupling process when the decay mode $n_s(\omega_s, \mathbf{k}_s)$ has an oscillation frequency. In this situation, two sidebands cannot satisfy the same dispersion relation simultaneously. The frequency-upshifted sideband $\mathbf{E}_1'(\omega_1', \mathbf{k}_1')$ is off resonant with the plasma and can be ignored in the coupling.

The most effective parametric instabilities excited directly by the HF heater are 1) parametric decay instability (PDI) and 2) oscillating two-stream instability (OTSI), in both mid-latitude and high-latitude regions [3–5]. The sideband(s) in mid-latitude region is Langmuir wave. In high-latitude region the sideband(s) can be upper hybrid wave or Langmuir wave, however, the instabilities involving Langmuir wave as a sideband have to compete with those excited in the upper hybrid resonance region, where the upper hybrid waves are the sidebands of the instabilities. The wavenumber k_0 of the heater is much smaller than the wavenumbers of the electrostatic sidebands and decay modes, thus a dipole pump, i.e., $\mathbf{k}_0 = 0$, is generally assumed.

3.1. Formulation of Parametric Couplings

Parametric excitation of Langmuir/upper hybrid waves $\phi(\omega, \mathbf{k})$ and low-frequency plasma waves $n_s(\omega_s, \mathbf{k}_s)$ by electromagnetic or Langmuir/upper hybrid pump waves $\mathbf{E}_p(\omega_0, \mathbf{k}_p)$ are considered in the following, where $\mathbf{E}_p$, ϕ, and n_s denote electric field of a pump wave, electrostatic potential of the Langmuir/upper hybrid sideband, and density perturbation of the low frequency decay mode, respectively. Langmuir waves can have large oblique propagation angles (with respect to the geomagnetic field $\mathbf{B}_0 = \hat{\mathbf{z}}B_0$), upper hybrid waves have near 90° propagation angles, and low-frequency plasma waves include ion acoustic/lower hybrid waves, and purely growing modes.

The coupled mode equation for the Langmuir/upper hybrid sideband is derived from the electron continuity and momentum equations, and Poisson's equation

$$\partial_t n_e + \nabla \cdot n_e \mathbf{v}_e = 0 \tag{3}$$

$$(\partial_t + \nu_e) n_e \mathbf{v}_e + \Omega_e n_e \mathbf{v}_e \times \hat{\mathbf{z}} = -\nabla \cdot n_e \mathbf{v}_e \mathbf{v}_e - 3v_{te}^2 \nabla \delta n_e - (e/m_e) n_e \mathbf{E} \tag{4}$$

$$\nabla^2\phi = 4\pi e\delta n_e \tag{5}$$

where $n_e = n_0 + \delta n_e + n_s$; n_0 and δn_e are the unperturbed plasma density and electron density perturbation associated with Langmuir/upper hybrid waves, respectively; $\Omega_e = eB_0/m_e c$ the electron cyclotron frequency; $v_{te} = (T_e/m)^{1/2}$ the electron thermal speed; $\mathbf{E} = \mathbf{E}_P + \mathbf{E}_L$ and $\mathbf{E}_L = -\nabla\phi$; and the adiabatic relationship $\nabla P_e = 3T_e\nabla\delta n_e$ is used; $\nu_{et} = \nu_{en} + \nu_{ei} + \nu_{eL} = \nu_e + \nu_{eL}$ is the effective electron collision frequency, where $\nu_e = \nu_{en} + \nu_{ei}$, ν_{en} is the electron-neutral elastic collision frequency, ν_{ei} the electron-ion Coulomb collision frequency [$\nu_{ei} = 2.632(n_0/T_e^{3/2})\ln\Lambda \cong 39.5(n_0/T_e^{3/2}) \cong 4.87\times10^{-7}(f_p^2/T_e^{3/2})$, here $\ln\Lambda \cong 15$ is assumed; n_0 is in cm^{-3}, T_e is in K, and f_p is the electron plasma frequency] and ν_{eL} a phenomenological collision frequency to model the electron Landau damping effect [$\nu_{eL} = (\pi/2)^{1/2}(\omega_a^2\omega_p^2/k_z k^2 v_{te}^3)\exp(-\omega_a^2/2k_z^2v_{te}^2)$; where ω_a is the plasma wave frequency, i.e., $\omega_a = \omega$ and $\nu_{et} = \nu_{eh}$ for the high frequency sideband and $\omega_a = \omega_s$ and $\nu_{et} = \nu_{es}$ for the low frequency decay mode].

With the aid of (5) and the following two orthogonal components of (4),

$$(\partial_t + \nu_{eh})n_e\mathbf{v}_e\times\hat{\mathbf{z}} = \Omega_e n_e\mathbf{v}_{e\perp} - \boldsymbol{\nabla}\cdot n_e\mathbf{v}_e\mathbf{v}_e\times\hat{\mathbf{z}} - [3v_{te}^2\nabla\delta n_e + (e/m_e)n_e\mathbf{E}]\times\hat{\mathbf{z}} \tag{6}$$

and

$$(\partial_t + \nu_{eh})n_e\mathbf{v}_{ez} = -\nabla\cdot n_e\mathbf{v}_e\mathbf{v}_{ez} - \left[3v_{te}^2\nabla_z\delta n_e + (e/m_e)n_e\mathbf{E}_z\right]$$

the three orthogonal components of (4) are combined into a single scalar equation

$$\begin{aligned}
&(\partial_t + \nu_{eh})\left[(\partial_t+\nu_{eh})^2 + \Omega_e^2\right]\nabla\cdot n_e\mathbf{v}_e \\
&= -\left[(\partial_t+\nu_{eh})^2+\Omega_e^2\right]\left[3v_{te}^2\nabla^2\delta n_e - \omega_p^2\delta n_e\right] + \Omega_e^2\nabla_\perp^2\left[3v_{te}^2\delta n_e - (e/m_e)\,n_0\phi\right] \\
&\quad -\left[\Omega_e^2\partial_z\nabla\cdot n_e\mathbf{v}_e v_{ez} + \Omega_e\,(\partial_t+\nu_{eh})\,\nabla\cdot\hat{\mathbf{z}}\times(\nabla\cdot n_e\mathbf{v}_e\mathbf{v}_e) + (\partial_t+\nu_{eh})^2\nabla\cdot(\nabla\cdot n_e\mathbf{v}_e\mathbf{v}_e)\right] \\
&\quad -(e/m_e)\left\{\left[(\partial_t+\nu_{eh})^2\nabla + \Omega_e^2\nabla_z\right]\cdot(n_s\mathbf{E}_P) - \Omega_e(\partial_t+\nu_{eh})\hat{\mathbf{z}}\cdot(\boldsymbol{\nabla}n_s\times\mathbf{E}_P)\right\}
\end{aligned} \tag{7}$$

where $\omega_p = (4\pi n_0 e^2/m_e)^{1/2}$ is the electron plasma frequency.

The right hand side (RHS) of (7) is assembled into four groups. The first two groups contain linear response terms and the last two contain coupling terms. The contribution to the parametric coupling from the third group is much smaller than that from the fourth group and hence, the coupling terms in the third group will be neglected. Use (3), (5), and (7), the coupled mode equation for the Langmuir (or upper hybrid) sideband is derived to be [6]

$$\begin{aligned}
&\left\{\left[(\partial_t+\nu_{eh})^2+\Omega_e^2\right]\left(\partial_t^2 + \nu_{eh}\partial_t + \omega_p^2 - 3v_{te}^2\nabla^2\right)\nabla^2 - \Omega_e^2\left(\omega_p^2 - 3v_{te}^2\nabla^2\right)\nabla_\perp^2\right\}\phi \\
&= \omega_p^2\left\{\left[(\partial_t+\nu_{eh})^2\nabla + \Omega_e^2\nabla_z\right]\cdot\langle\mathbf{E}_p n_s^*/n_0\rangle - \Omega_e(\partial_t+\nu_{eh})\hat{\mathbf{z}}\cdot\langle\nabla(n_s^*/n_0)\times E_P\rangle\right\}
\end{aligned} \tag{8}$$

where $\langle\,\rangle$ stands for a filter, which keeps only terms having the same phase function as that of the function ϕ on the left hand side. Although (8) is derived from the fluid equations, the kinetic effect of electron Landau damping has been added phenomenological in the collision damping rate.

Both electrons and ions respond effectively to low frequency wave fields, hence the formulation of the coupled mode equation involve electron and ion fluid equations. Because electrons and ions tend to move together, the formulation can be simplified by introducing quasi-neutral condition: $n_{si} \cong n_{se} = n_s$. The ion fluid equations are similar to (3) and (4), except that the subscript e is changed to i, and the charge $-e$ changed to e. Moreover, the collision terms $\nu_e\mathbf{v}_e$ and $\nu_i\mathbf{v}_i$ are replaced by $\nu_{ei}(\mathbf{v}_e - \mathbf{v}_i)$ and $\nu_{ie}(\mathbf{v}_i - \mathbf{v}_e) + \nu_{in}\mathbf{v}_i$ in the electron and ion fluid equations, respectively, where ν_{in} is the ion-neutral collision frequency. The ion Landau damping rate $\nu_{iL}/2 \cong (\pi/8)^{1/2}(\omega_s^2/k_z v_s)(T_e/T_i)^{3/2}\exp(-\omega_s^2/2k_z^2v_{ti}^2)$ on the ion acoustic wave will be included through a phenomenological collision frequency in the ion acoustic wave coupled mode equation by replacing ν_{in} by $\nu_{in} + \nu_{iL} = \nu_i$, where $v_s = (T_e/M)^{1/2}$. Also included in the formulation is the electron thermal energy equation [7]

$$\partial_t T_e + (2T_{e0}/3)\,\nabla\cdot\mathbf{v}_e = (2/3n_e)\nabla\cdot(\kappa_z\nabla_z + \kappa_\perp\nabla_\perp)T_e - 2\nu_e(m/M)\,(T_e - T_{e0}) + 2\nu_e m\left\langle v_e^2\right\rangle/3 \tag{9}$$

where $\kappa_z = 3n_0T_{e0}/2m\nu_e$, $\kappa_\perp = (\nu_e/\Omega_e)^2\kappa_z$, and T_{e0} is the unperturbed electron temperature.

Using the same procedure as that outlined in the early work [8], the coupled mode equation for the low frequency mode in the collision case is derived to be

$$\begin{aligned}
&\left\{\partial_t^3\left\{(\partial_t+\nu_{es})\left[\partial_t(\partial_t+\nu_i)-C_s^2\nabla^2\right]+\Omega_e\Omega_i\partial_t\right\}\nabla_\perp^2\right.\\
&\left.+\Omega_e^2\left\{\left(\partial_t^2+\Omega_i^2\right)\left[\partial_t(\partial_t+\nu_i)-C_s^2\nabla^2\right]+\Omega_i^2C_s^2\nabla_\perp^2\right\}\nabla_z^2\right\}(n_s/n_0)\\
=\;&(m/M)\left[\left(\partial_t^2+\Omega_i^2\right)\nabla_z^2+\partial_t^2\nabla_\perp^2\right]\left[\partial_t(\partial_t+\nu_{es})\nabla_\perp\cdot(\mathbf{a}_{p\perp}+\nabla_\perp\delta T_e/m)\right.\\
&\left.+\Omega_e^2(\partial_z a_{pz}-\partial_t\nabla\cdot\mathbf{J}_B/n_0)-\Omega_e\partial_t\nabla\cdot\mathbf{a}_p\times\hat{\mathbf{z}}\right]
\end{aligned}\tag{10}$$

where Ω_i is the ion cyclotron frequency, $C_s=[(T_e+3T_i)/M]^{1/2}$ the ion acoustic speed, $v_{ti}=(T_i/M)^{1/2}$ the electron thermal speed, and M the ion (O^+) mass; the coupling terms $\mathbf{a}_p=\langle\mathbf{v}_e\cdot\nabla v_e\rangle$ and $\mathbf{J}_B=\langle n_e\mathbf{v}_e\rangle$ arise from plasma nonlinearities and can be expressed explicitly by taking the linear part of the electron velocity response and the electron density response to the high frequency wave fields; and $\delta T_e=T_e-T_{e0}$ is the result of the differential Ohmic heating, which is significant only for the field-aligned purely-growing modes and can be evaluated from (9). In the analyses, (8) and (10) can be simplified for each considered parametric coupling process before being linearized and transformed to the k-ω domain; the spatial and temporal variation of physical functions in (8) and (10) are assumed to have the form of $p=p\exp[i(\boldsymbol{\kappa}\cdot\mathbf{r}-\varpi t)]$. Thus (8) and (10) are converted to the coupled algebraic equations, which are combined to derive the dispersion equation of a parametric instability, where $\boldsymbol{\kappa}$ and $\varpi=\varpi_r+\mathbf{i}\mathbf{r}$ are the appropriate wavevector and complex frequency of each physical quantity.

3.2. Analyses

Exemplified in the following are the decay of an O-mode EM dipole pump $\mathbf{E}_p(\omega_0,\,\mathbf{k}_p=0)$ into a Langmuir/upper hybrid sideband $\phi(\omega,\,\mathbf{k})$ and an ion acoustic/lower hybrid decay mode $n_s(\omega_s,\,\mathbf{k}_s)$ in the spatial region below the HF reflection height, where $\mathbf{E}_p=(\hat{\mathbf{x}}+i\hat{\mathbf{y}})E_{p\perp}+\hat{\mathbf{z}}E_{pz}+$ c.c.; $E_{p\perp,z}=(\varepsilon_{p\perp,z}/2)\exp(-i\omega_0t)$ and c.c. represents complex conjugate; thus, $\mathbf{E}_p=\hat{\mathbf{z}}E_p+\text{c.c.}=\hat{\mathbf{z}}\varepsilon_p\cos\omega_0t$ near the HF reflection height and $\mathbf{E}_p=(\hat{\mathbf{x}}-i\hat{\mathbf{y}})E_p+\text{c.c.}=\varepsilon_p(\hat{\mathbf{x}}\cos\omega_0t-\hat{\mathbf{y}}\sin\omega_0t)$ in the high-latitude upper hybrid resonance region; ϕ and n_s denote the sideband's electrostatic potentials and ion acoustic/lower hybrid mode's density perturbation, respectively; $\mathbf{k}=\hat{\mathbf{z}}k_z+\hat{\mathbf{x}}k_\perp$; frequency and wavevector matching conditions lead to $\omega=\omega_0-\omega_s^*$ and $\mathbf{k}_s=-\mathbf{k}$.

3.2.1. Oscillating Two-stream Instability (OTSI)

3.2.1.1 Excitation of Langmuir Waves Together with Purely Growing Density Striations

From (8), the coupled mode equations for Langmuir sidebands $\phi_1(\omega_1,\,\mathbf{k}_1)$ and $\phi_1'(\omega_1',\,\mathbf{k}_1')$ are

$$\begin{aligned}
&\left\{\left[(\partial_t+\nu_{eh})^2+\Omega_e^2\right]\left(\partial_t^2+\nu_{eh}\partial_t+\omega_p^2-3v_{te}^2\nabla^2\right)\nabla^2-\Omega_e^2(\omega_p^2-3v_{te}^2\nabla^2)\nabla_\perp^2\right\}\phi_{1\pm}\\
&=\omega_p^2[(\partial_t+\nu_{eh})^2+\Omega_e^2]\partial_z\langle E_pn_{s\pm}/n_0\rangle
\end{aligned}\tag{11}$$

where the notations $\phi_{1+}=\phi_1$, $\phi_{1-}=\phi_1'$, and $n_{s+}^*=n_s=n_{s-}$ are used.

The parallel (to the magnetic field) component of the wavevector of the short scale purely growing mode is not negligibly small, thus the short scale purely growing mode, similar to the ion acoustic mode, is also mainly driven by the parallel component of the ponderomotive force induced by the high frequency wave fields. The coupled mode Equation (10) for the purely growing mode is reduced to

$$\left\{\left(\partial_t^2+\Omega_i^2\right)\left[\partial_t(\partial_t+\nu_{in})-C_s^2\nabla^2\right]+\Omega_i^2C_s^2\nabla_\perp^2\right\}\nabla_z^2(n_s/n_0)=(m/M)\left[\left(\partial_t^2+\Omega_i^2\right)\nabla_z^2+\partial_t^2\nabla_\perp^2\right]\partial_z a_{pz}\tag{12}$$

where $a_{pz}=\partial_z\langle v_{ez}^2/2\rangle$ for the present case that $\mathbf{E}_p=\hat{\mathbf{z}}E_p+\text{c.c.}$.

Equations (11) and (12) are transformed to the k-ω domain and combined to a dispersion equation

$$\begin{aligned}
&\left\{\left(\gamma_s^2+\Omega_i^2\right)\left[\gamma_s(\gamma_s+\nu_{in})+k_1^2C_s^2\right]-\Omega_i^2k_\perp^2C_s^2\right\}\\
&=2\left(e^2/mM\right)k_1^2\cos^2\theta\left(\gamma_s^2+\Omega_i^2\cos^2\theta\right)\left\{\Delta\omega^2/\left[\Delta\omega^4+\omega_0^2(2\gamma_s+\nu_{eh})^2\right]\right\}|E_p|^2,
\end{aligned}\tag{13}$$

where $\Delta\omega^2=\omega_p^2+3k_1^2v_{te}^2+\Omega_e^2\sin^2\theta-\omega_0^2$, and $\theta=\sin^{-1}(k_\perp/k_1)$.

We first set $\gamma_s = 0$ in (13) to determine the threshold condition of the instability. The threshold field is obtained to be

$$\varepsilon_{pth} = 2|E_p(\theta)|_{th} = \left(2mM/e^2\right)^{1/2} C_s \left[\left(\Delta\omega^4 + \omega_0^2\nu_{eh}^2\right)/\Delta\omega^2\right]^{1/2} / \cos\theta. \tag{14}$$

Equation (14) shows that the threshold field of OTSI varies with the propagation angle θ and wavelength λ_1 of the Langmuir sidebands as well as the location of excitation. For each propagation angle θ and wavelength λ_1, the instability has the minimum threshold field

$$\varepsilon_{pthm} = 2|E_p(k_1,\theta)|_m = 2\left(mM/e^2\right)^{1/2} C_s \left(\omega_0\nu_{eh}\right)^{1/2} / \cos\theta \tag{15}$$

when it is excited in a preferential layer at height h, with $\omega_p^2(h) = \omega_p^2(k_1,\theta) = \omega_0(\omega_0 + \nu_{eh}) - 3k_1^2v_{te}^2 - \Omega_e^2\sin^2\theta$, i.e., $\Delta\omega^2(k_1,\theta) = \omega_0\nu_{eh}$. In other words, the spectral lines of the Langmuir sidebands excited by OTSI have an angular (θ) and a spectral (k_1) distribution, as well as a spatial (h) distribution in a finite altitude region. This minimum threshold field (15) increases with the oblique propagation angle θ of (k_1, θ) lines, but it is independent of k_1. The altitude h of the preferentially excited region for (k_1, θ) lines moves downward as the oblique propagation angle θ of these lines increases.

The maximum growth rate $\gamma_{sM}(k_1,\theta)$ of the instability and its excitation region are determined by taking partial derivative of $\Delta\omega^2$ on (13) and setting $\partial\gamma_s/\partial\Delta\omega^2 = 0$ in the resultant. It leads to $\Delta\omega^2|_m = \Delta\omega'^2(k_1,\theta) = \omega_0(2\gamma_{sM} + \nu_{eh})$, and $\gamma_{sM}^3 + \gamma_{sM}k_1^2C_s^2 - (\nu_{eh}k_1^2C_s^2/2)(|E_p|^2/|E_p(k_1,\theta)|_m^2) \cong 0$, where $\gamma_{sM}^2 \gg \Omega_i^2$, ν_{eh}^2 are assumed (i.e., $|E_p|^2/|E_p(k_1,\theta)|_m^2 \gg 1$). This quadratic equation for γ_{sM} has a real solution

$$\gamma_{sM} = (G+H)^{1/3} - (G-H)^{1/3}, \tag{16}$$

where $G = [(k_1^2C_s^2/3)^3 + H^2]^{1/2}$ and $H = (\nu_{eh}k_1^2C_s^2/4)(|E_p|^2/|E_p(k_1,\theta)|_m^2)$.

The RHS of (16) can be simplified in two pump power regimes. In the moderate heating power regime that $|E_p|^2/|E_p(k_1,\theta)|_m^2 < 2k_1C_s/\nu_{eh}$ (i.e., $\gamma_{sM} < k_1C_s$), (16) reduces to $\gamma_{sM} \sim (\nu_{eh}/2)(|E_p|^2/|E_p(k_1,\theta)|_m^2)$. On the other hand, it reduces to $\gamma_{sM} \sim (2H)^{1/3}$ in the strong power regime that $|E_p|^2/|E_p(k_1,\theta)|_m^2 > 2k_1C_s/\nu_{eh}$ (i.e., $\gamma_{sm} > k_1C_s$). It is noted that the altitude h_1' of the maximum growth rate layer (i.e., $\omega_p^2(h_1') = \omega_p^2(h_1) + 2\omega_0\gamma_{sM}$) is slightly higher than the altitude h_1 of the minimum threshold layer (i.e., $h_1' > h_1$). The height difference is given by $\Delta h = h' - h \cong 2\gamma_{sM}L/\omega_0$, where L is the linear scale length of the plasma density distribution. It shows that the height of the preferential (maximum growth rate) layer of the instability tends to shift upward from the matching height of the instability sidebands as the heating power (i.e., γ_{sM}) increases. However, in the moderate power regime this shift is negligibly small.

3.2.1.2 Excitation of Upper Hybrid Waves $\phi_{1\pm}$ ($(\omega_1, \pm k_1)$ Together with Field-aligned Density Irregularities n_s ($\omega_s = i\gamma_s$, $k_s = -\mathbf{k}_1$)

Under the assumption that $|k_z/k_\perp| \sim 0$, the dispersion equation is derived from combining (8) and (10) to be

$$\begin{aligned}&\left[\left(\gamma_s + 2\nu_e m/M + \nu_e k_1^2 v_{te}^2/\Omega_e^2\right)\left(\gamma_s\Omega_e\Omega_i/\nu_{es} + k_1^2C_s^2\right) + \gamma_s k_1^2C_s^2/3\right]\left(\omega_0^2\nu_{eh}^2 + \Gamma^2\right)\\ &= 2\nu_{eh}\left(4e^2/3mM\right)k_1^2(1-\Omega_e/\omega_0)^2\left[\Gamma - \nu_{eh}^2 - \omega_0^2k_1^2/2k_D^2\right]|E_p|^2\end{aligned} \tag{17}$$

where $\Gamma = \omega_{uk}^2 - \omega^2$, $\omega_{uk}^2 = \omega_u^2 + 3k_1^2v_{te}^2$, $\omega_u^2 = \omega_p^2 + \Omega_e^2$, and $k_D = \omega_p/v_{te}$.

Set $\gamma_s = 0$ in (17), the threshold field $\varepsilon_{pth} = 2|E_p|_{th}$ of the instability is obtained to be

$$\varepsilon_{pth} = 2(C_s/e)\left[3mM\left(\omega_0^2\nu_{eh}^2 + \Gamma^2\right)\left(2m/M + k_1^2v_{te}^2/\Omega_e^2\right)/8\left(1-\Omega_e/\omega_0\right)^2\left(\Gamma - \nu_{eh}^2 - \omega_0^2k_1^2/2k_D^2\right)\right]^{1/2} \tag{18}$$

The right hand side of (18) has to be positive, it leads to the condition that

$$\Gamma > \nu_{eh}^2 + \omega_0^2k_1^2/2k_D^2 = a \tag{19}$$

The threshold field for $\Gamma = \Gamma_0 = a + (a^2 + \nu_e^2\omega_0^2)^{1/2}$ has the minimum value

$$\varepsilon_{pthm} = 2(C_s/e)\left[3mM\left(\omega_0^2\nu_{eh}^2 + \Gamma_0^2\right)(2m/M + k_1^2v_{te}^2/\Omega_e^2)/8(1-\Omega_e/\omega_0)^2(a^2 + \nu_{eh}^2\omega_0^2)^{1/2}\right]^{1/2} \tag{20}$$

The growth rate of the instability is obtained from (17) to be

$$\gamma_S = (\nu_{eh}/2)\left\{[b^2 + 8(k_1^2 v_{te}^2/\Omega_e^2)(2m/M + k_1^2 v_{te}^2/\Omega_e^2)(|\varepsilon_P/\varepsilon_{pthm}|^2 - 1)]^{1/2} - b\right\} \tag{21}$$

where $b = 2m/M + 11k_1^2 v_{te}^2/3\Omega_e^2$.

3.2.2. Parametric Decay Instabilities (PDI)

3.2.2.1 Decay to Langmuir and Ion Acoustic Waves

The dispersion equation is derived to be

$$\begin{aligned}&\left[\omega^2 + i\nu_{eh}\omega - \omega_{k\theta}^2\right]\left[1 + \left(1 - \Omega_e^2/\omega^2\right)^{-1}\left(\Omega_e^2/\omega^2\right)\sin^2\theta\right]\left[\omega_s^*\left(\omega_s^* - i\nu_i\right) - k^2 C_s^2\right]\\ &= \omega_p^2 (e/m\omega)^2 (m/M)\left\{1 + \left(1 - \Omega_e^2/\omega^2\right)^{-1}\left[\omega_s\left(\omega_u^2 - \omega^2\right)/\omega_p^2\omega\right]\tan^2\theta\right\}\left[(k_z|E_{pz}|)\right.\\ &\left. + (1 + \Omega_e/\omega)^{-1}(k_\perp|E_{p\perp}|)\right]^2\end{aligned} \tag{22}$$

where $\omega_{k\theta}^2 = \omega_p^2 + 3k^2 v_{te}^2 + \Omega_e^2 \sin^2\theta$ and $\sin^2\theta = k_\perp^2/k^2$.

We now set $\omega = \omega_r + i\gamma_k$ and $\omega_s = \omega_{sr} + i\gamma_k$ in (22) to evaluate the threshold field $\varepsilon_{pth} = 2E_{pth}(k, \theta)$ and growth rate $\gamma_k(\theta)$ of the instability excited at an arbitrary height h_1, where $\omega_p^2(h_1) = \omega_r^2 - 3k_1^2 v_{te}^2 - \Omega_e^2 \sin^2\theta_1$ is the matching height of the (k_1, θ_1) Langmuir wave. In the general case that when the sideband and decay wave of the instability are driven waves excited near the HF reflection height, rather than eigen-modes of plasma, the threshold field and growth rate of the instability are obtained to be

$$|E_{pth}(k, \theta; k_1, \theta_1)| = \left(1 + \Delta\omega_1^4/\omega_0^2\nu_{eh}^2\right)^{1/2}(\mathrm{mM}/e^2)^{1/2}\left(\nu_{eh}\nu_i\omega_{sr}\omega_0^3\right)^{1/2}/k\cos\theta\omega_p \tag{23}$$

and

$$\gamma_k \cong \left[(\nu_{eh}\nu_i/4)\left(E_p/E_{pth}\right)^2 + (\nu_{eh} - \nu_i)^2/16\right]^{1/2} - (\nu_{eh} + \nu_i)/4 \tag{24}$$

where $\Delta\omega_1^2 = \omega_{k\theta}^2 - \omega_r^2 = 3(k^2 - k_1^2)v_{te}^2 + \Omega_e^2(\sin^2\theta - \sin^2\theta_1)$; $\omega_{sr}^2 = k^2 C_s^2 - \omega_{sr}\nu_i\Delta\omega_1^2/\omega_r\nu_{eh}$.

It is shown in (23) that the threshold field also varies with the propagation angle θ and wavelength λ_1 of the Langmuir sideband as well as the location of excitation. When the instability is excited at the matching height h of its Langmuir sideband (k, θ) in the region between the HF reflection height and the upper hybrid resonance layer, i.e., $\Delta\omega_1 = 0$, the threshold field is the minimum given by

$$\begin{aligned}\varepsilon_{pthm} &= 2\left|E_{pth}(k, \theta)\right|_m \cong 2\left(\mathrm{mM}/e^2\right)^{1/2}\left(1 - \Omega_e^2\sin^2\theta/\omega_0^2\right)^{-1/2}\left[1 + \left(1 - \Omega_e^2/\omega_0^2\right)^{-1}\left(\omega_{sr}/\omega_p^2\omega_0\right)\right.\\ &\left.\times(\Omega_e^2\cos^2\theta - 3k^2 v_{te}^2)\tan^2\theta\right]^{-1/2}(\nu_{eh}\nu_i\omega_{sr}\omega_0^3)^{1/2}/\omega_p k\cos\theta\end{aligned} \tag{25}$$

3.2.2.2 Decay to Upper Hybrid Wave $\phi(\omega, k)$ and Lower Hybrid Wave $n_s(\omega_s, k_s = -k)$

Use the similar approach to combine (8) and (10), under the condition $|k_z/k_\perp| \ll 1$, it yields a dispersion equation

$$(-\Gamma + i\nu_e\omega)\left[\omega_s{}^{*2} - i(\nu_{es} + \nu_i/\xi)\omega_s^* - \omega_{Lks}^2\right] \cong \left(e^2/mM\right)(\Omega_e/\omega_0)^2\left[3k^2 v_{te}^2/\omega_s^*(\omega_0 + \Omega_e)\right]k^2|E_p|^2 \tag{26}$$

where $\Gamma = \omega_{uk}^2 - \omega^2$; $\omega_{Lks}^2 = \omega_{LH}^2\xi + k^2 C_s^2$, $\omega_{LH}^2 = \omega_{pi}^2/(1 + \omega_p^2/\Omega_e^2) \cong \Omega_e\Omega_i$ and $\xi = 1 + (M/m)(k_z^2/k_\perp^2)$; $\nu_e = \nu_{ei} + \nu_{en}$, $\nu_{es} = \nu_e + \nu_{eLs}$, and $\nu_{eLs} = (\pi/2)^{1/2}(M/m)^{3/2}[\omega_{LH}^4\xi/k^3 v_{te}^3(\xi - 1)^{1/2}]\exp[-M\omega_{LH}^2\xi/2mk^2 v_{te}^2(\xi - 1)]$. We now set $\omega = \omega_{uk} + i\gamma_k$ and $\omega_s = \omega_{Lks} + i\gamma_k$ in (26) and evaluate the threshold field $\varepsilon_{pth} = 2e_{0th}$ and the growth rate γ_k of the instability excited in upper hybrid resonance region. Thus (26) reduces to

$$(2\gamma_k + \nu_e)(2\gamma_k + \nu_{es} + \nu_i/\xi) = (e/m\omega_0^2)^2(1 + \Omega_e/\omega_0)^{-1}\left(3k^2 v_{te}^2/\xi\right)k^2|E_p|^2 \tag{27}$$

and E_{pUth} and γ_{kU} of the instability are determined to be

$$|E_{pU}|_{th} = (m/e)\,(1+\Omega_e/\omega_0)^{1/2}\,[\nu_e\,(\nu_{es}+\nu_i/\xi)]^{1/2}\,(\xi/3)^{1/2}\left(\omega_0^2/k_1^2 v_{te}\right) \tag{28}$$

and

$$\gamma_{kU} = \left\{[\nu_e(\nu_{es}+\nu_i/\xi)/4]\,(E_p/E_{pUth})^2 + (\nu_e-\nu_{es}-\nu_i/\xi)^2/16\right\}^{1/2} - (\nu_e+\nu_{es}+\nu_i/\xi)/4 \tag{29}$$

3.2.3. Langmuir Cascade

Langmuir waves excited by OTSI and PDI in the region below the HF reflection height can become pump waves to excite new parametric instabilities, which generate frequency-downshifted Langmuir waves to be their sidebands. This is called "Langmuir cascade". Continuous cascade of Langmuir waves through new parametric instabilities broadens the downshifted frequency spectrum of Langmuir waves [9, 10]. Similar description is also applicable to the "upper hybrid cascade". The permissible number of cascade and the required pump threshold field vary with each cascade process characterized by the low frequency decay mode. In the following, a Langmuir cascade process that involves an ion acoustic wave as the decay mode is discussed. This three-wave coupling process is represented by

$$\text{Langmuir Pump } (\mathbf{k}_1,\omega_1) \rightarrow \text{Langmuir sideband } (\mathbf{k}_2,\omega_2) + \text{Ion acoustic wave } (\mathbf{k}_s,\omega_s)$$

where $\mathbf{k}_2 = \mathbf{k}_1 - \mathbf{k}_s$ and $\omega_2 = \omega_1 - \omega_s^*$.

Because HFPLs have a fixed k value, the cascade lines in the HFPLs are originated from different heights, moving down sequentially. In the frequency spectrum of HFPLs, the first spectral peak having the highest frequency at $\omega = \omega_1$ is an OTSI line if $\omega_1 = \omega_0$, the heating wave frequency; if ω_1 is downshifted from ω_0 by $\Delta\omega = \omega_0 - \omega_1 = \omega_{S_0} = 2k_R C_s$, where k_R is the wavenumber of the probing backscatter radar signal, then it is a PDI line; the subsequent spectral peaks at ω_2, ω_3, ... correspond to the first, second, ... cascade lines. The cascade lines are recognized by doubling their frequency downshift from the preceding lines to $2\omega_{S_0}$. For example, if a spectrogram of HFPLs contains 7 spectral peaks starting at $\omega = \omega_0$, then the first two spectral peaks at $\omega = \omega_0$ and $\omega_0 - \omega_{S_0}$ are called OTSI and PDI line, respectively. The remaining 5 spectral peaks at $\omega_0 - (2n+1)\omega_{S_0}$, $n = 1, \ldots, 5$ are called cascade lines and are attributed to the PDI process. Therefore, the spectral width of HFPLs is about $11\omega_{S_0}$.

3.2.4. Filamentation Instability

A large-amplitude wave propagating in plasma can breakup into filaments because of the filamentation instability [11]. This occurs from small perturbations of the plasma density, which result in a modulation of the plasma dielectric constant and wave distribution. This in turn increases the density perturbation. Filamentation instability can be excited by the HF heater directly, that is termed electromagnetic filamentation instability [12], as well as by the plasma waves (such as Langmuir wave and upper hybrid wave), that is termed electrostatic filamentation instability [6].

Similar to the OTSI, filamentation instability is also a four-wave coupling process involving purely growing decay mode. The differences are that the spatial variation of the purely growing decay mode in the filamentation instability is in the direction perpendicular, rather than parallel, to the wave propagation direction and its scale length is much larger than that of the purely growing decay mode excited by the OTSI. The purely growing decay modes of filamentation instabilities are either directly excited in field-aligned nature (i.e., varying spatially in the direction perpendicular to the background magnetic field) or evolved, after excitation, into field-aligned nature, which are termed field-aligned density irregularities (FAIs). Short to medium scale (i.e., less than 100 meters) FAIs cause intense bistatic scattering and backscattering of ground-based HF/VHF/UHF radar signals [13]. The large scale FAIs (i.e., larger than a few hundred meters) cause virtual height spread of the sounding echoes in the ionogram, known as (artificial) spread-F, and scintillation of the beacon satellite signals [14].

In HF heating experiments, HF heaters generate large-scale FAIs directly via electromagnetic filamentation instability [12, 15, 16]. Sheet-like large-scale FAIs [17] were observed. Those in short to medium scale sizes are generated via electrostatic filamentation instabilities [6], which are excited by the high frequency sidebands of the PDI and OTSI.

4. NONLINEAR SCHRODINGER EQUATION FOR LANGMUIR WAVES

Near the O-mode reflection height, the pump wave and the dominant parts of parametrically excited plasma waves are polarized in parallel and nearly parallel to the geomagnetic field. In essence, these waves evolve in unmagnetized plasma. In the following, unmagnetized fluid equations will be combined into two; one describes the Langmuir wave and the other one for the ion wave, which are coupled to each other due to the nonlinear nature of the plasma. We will introduce some assumptions and make approximations accordingly to combine these two equations into a single one describing the nonlinear Langmuir waves.

4.1. Coupled Nonlinear Equation for the Langmuir Wave

The coupled mode equation for the Langmuir wave is derived from (3) to (5), in which the magnetic field term (the second term on the LHS) of (4) is removed and (5) is rewritten as

$$\nabla \cdot \mathbf{E} = -4\pi e(n_e - \hat{\mathbf{n}}) = -4\pi e\delta n_e \tag{30}$$

where $n_e = n_0 + \delta n_e + n_s$; $\hat{\mathbf{n}} = n_0 + n_s$; n_0, δn_e, and n_s are the unperturbed plasma density and electron density perturbations associated with Langmuir waves and ion waves, respectively. Apply the operation $(\partial_t + \nu_e)$ to (3), i.e., $(\partial_t + \nu_e)$ (3), and with an aid of (4), we obtain

$$\partial_t(\partial_t + \nu_e)\delta n_e - \nabla \cdot (3v_{te}^2 \nabla \delta n_e) = \langle \nabla \cdot (\nabla \cdot n_e \mathbf{v}_e \mathbf{v}_e) + (e/m_e)\nabla \cdot (n_e \mathbf{E}) \rangle \tag{31}$$

where $\langle\ \rangle$ stands for a filter, which keeps only terms in the same frequency range. Thus,

$$\langle \nabla \cdot (n_e \mathbf{E}) \rangle = n_0 \nabla \cdot \mathbf{E} + \nabla \cdot (n_s \mathbf{E}) \tag{32}$$

Substitute (32) into (31) and with the aid of (30), a governing equation for the Langmuir wave field $\mathbf{E}$ is derived to be

$$\left[\partial_t \left(\partial_t + \nu_e\right) + \omega_p^2 - 3v_{te}^2 \nabla^2\right] \mathbf{E} = -4\pi e \langle \nabla \cdot (n_e \mathbf{v}_e \mathbf{v}_e) \rangle - \left(\omega_p^2/n_0\right)(n_s \mathbf{E}) \tag{33}$$

This is the nonlinear mode equation of the Langmuir wave. The nonlinear nature of the equation is shown implicitly by the two terms on the RHS of (33). The second term on the RHS of (33) depends explicitly on the density perturbation of the ion wave and manifests the coupling between Langmuir waves and ion waves. Therefore, the equation for the ion wave is needed and derived.

4.2. Coupled Nonlinear Equation for the Ion Wave

We combine the momentum equations of electron and ion fluids by adding them together. The electric field terms and electron-ion collision terms in the two equations are cancelled; and the electron inertial term $m_e \partial_t \mathbf{v}_e$ and the ion convective term $m_i \mathbf{v}_i \cdot \nabla \mathbf{v}_i$, which are small comparing to their respective counterpart, can be neglected. The result is

$$m_i(\partial_t + \nu_{in})\ \mathbf{v}_i + \ m_e \mathbf{v}_e \cdot \nabla \mathbf{v}_e = -n_0^{-1} \nabla (P_e + P_i) \tag{34}$$

With the aid of the quasi-neutrality, the relation $\mathbf{v}_e \cdot \nabla \mathbf{v}_e = \nabla(v_e^2/2)$, and the continuity equation $\partial_t n_s + \nabla \cdot (n_0 \mathbf{v}_i) = 0$, (34) becomes

$$\left[\partial_t(\partial_t + \nu_{in}) - C_s^2 \nabla^2\right](n_s/n_0) = (m_e/m_i)\nabla^2 \left\langle \left(v_e^2/2\right) \right\rangle \tag{35}$$

where the implicit nonlinear term on the RHS of (35) can be expressed explicitly in terms of the Langmuir wave field E. In other words, through the nonlinearity of plasma, ion waves are driven by the Langmuir waves.

4.3. Assumptions and Approximations

Consider only low frequency off-resonant ion waves, which are directly driven by the Langmuir waves. We can assume that $|\partial_t(\partial_t + \nu_{in})(n_s/n_0)| \ll |C_s^2 \nabla^2 (n_s/n_0)|$ and (10) is approximated to obtain $(n_s/n_0) \cong -(m_e/m_i)\langle (v_e^2/2) \rangle / C_s^2$. Moreover, we will assume that $|\langle (\nabla \cdot (n_e \mathbf{v}_e \mathbf{v}_e) \rangle| \ll |(\omega_p^2/4\pi e n_0)(n_s \mathbf{E})|$. This assumption imposes an upper bound on the amplitude and lower bound on the scale length of a nonlinear Langmuir wave governed validly by the equation in the formulation. Thus (33) reduces to

$$\left[\partial_t(\partial_t + \nu_e) + \omega_p^2 - 3v_{te}^2 \nabla^2\right] E = \left(\omega_{pi}^2/C_s^2\right) \left\langle \left(v_e^2/2\right) \right\rangle E \tag{36}$$

4.4. Derivation of Nonlinear Schrodinger Equation for Langmuir Waves

Set $E = \varepsilon(\xi,\tau)\exp[-i(\omega_1 t - k_1 z)] + \text{c.c.}$, where $\xi = k_1 z - \tau$, $\tau = k_1 v_g t$, $v_g = \partial_k \omega|_{\omega 1,k1} = 3k_1 v_{te}^2/\omega_1$, and $\varepsilon(\xi, \tau)$ is the envelope of the wave, ω_1 and k_1 are the carrier frequency and wavenumber, and c.c. stands for complex conjugate, thus $v_e \cong -i[e\varepsilon(\xi,\tau)/m_e\omega_1]\exp[-i(\omega_1 t - k_1 z)] + \text{c.c.}$; and take forward wave approximation, (36) reduces to

$$-1/2\partial_\xi^2 a + \left(V_l - A|a|^2\right) a = i\partial_\tau a \tag{37}$$

where $a = e\varepsilon/m_e\omega_1 v_{te}$, $V_l = -\Delta\omega^2/6k_1^2 v_{te}^2$, $\Delta\omega^2 = \omega^2 - (\omega_p^2 + 3k^2 v_{te}^2)$, and $A = (\omega_{pi}^2/6k_1^2 C_s^2)$.

Equation (37) is a nonlinear Schrodinger equation, where the wave function $a(\xi, \tau)$ represents the envelope of Langmuir waves [18, 19]. The third term on the LHS of (37) is a cubic nonlinear term. In the Hamiltonian representation, this term, $V_l - A|a|^2$, represents a potential operator of the system, where V_l is a linear potential function and $-A|a|^2$ is a self-induced nonlinear potential function. The total potential function $(V_l - A|a|^2)$ varies with the intensity of the wave function, thus it is possible to trap the wave function in self-induced potential well. When this occurs, the package of Langmuir waves evolves into a localized nonlinear wave having an envelope called "Soliton" to be demonstrated in the following.

4.5. Analysis

Let $a(\xi,\tau) = F(\xi)e^{-i(\varpi\tau+\Phi)}$, where $F(\xi)$ is a real function, then (37) reduced to

$$F'' + \Lambda F + 2AF^3 = 0 \tag{38a}$$

where $F'' = d_\xi^2 F$ and $\Lambda = 2(\varpi - V_l)$.

Consider F as the spatial coordinate of an unit mass object in an one dimensional space, Equation (38a) represents an equation of motion of the object, in which the acceleration is given to be $-(\Lambda F + 2AF^3)$. This equation is integrated to be

$$1/2(F')^2 + 1/2\left(\Lambda F^2 + AF^4\right) = C_1 \tag{38b}$$

where the integration constant $C_1 = 1/2[F'^2(0) + \Lambda F^2(0) + AF^4(0)]$.

Equation (38b) is the energy conservation equation describing the trajectory of the object in the potential field $VE = 1/2(\Lambda F^2 + AF^4) = TE - KE$, where the total energy $TE = C_1$ and kinetic energy $KE = 1/2(F')^2$. Two typical plots of the potential function in the cases of $\Lambda > 0$ and $\Lambda < 0$ are exemplified in Fig. 3(a). As shown, both plots represent potential wells.

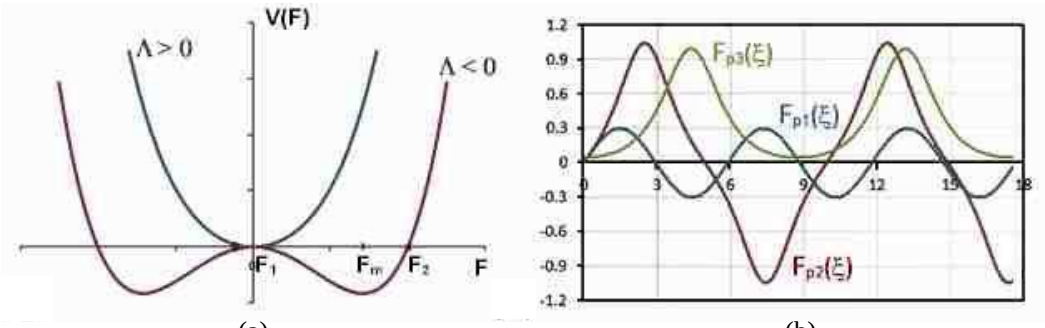

Figure 3. (a) Two potential distributions showing three type potential wells and (b) three periodic solutions corresponding to the three periodic trajectories trapped in the three type potential wells shown in (a).

In the case of $\Lambda > 0$, the potential well traps objects with $C_1 > 0$; the trapped object is bounced back and forth in the potential well to have a periodic trajectory $F_{p1}(\xi)$, illustrated in Fig. 3(b), which is a symmetric alternate function. In the case of $\Lambda < 0$, the potential well traps objects with $C_1 > 0$ as

well as with $1/2(\Lambda F_m^2 + AF_m^4) < C_1 < 0$. For $C_1 > 0$, the bounce motion of the object has a periodic trajectory $F_{p2}(\xi)$, which is a symmetric alternate function as illustrated in Fig. 3(b). On the other hand, as shown in Fig. 3(b), the periodic trajectory $F_{p3}(\xi)$ of the object for $1/2(\Lambda F_m^2 + AF_m^4) < C_1 < 0$ is a non-alternate function. Moreover, there is also exists a non-periodic trajectory for $C_1 = 0$ in the case of $\Lambda < 0$. Let the object start at $F = F_1(= 0)$ and exam the motion of the object in the region between F_1 and F_2. Initially, it moves very slowly to the right. As it drops into the potential well, it moves quickly toward the potential minimum at F_m. After passing the potential minimum, the object starts to climb up to the turning point at $F = F_2$, where the object is bounced back into the potential well. It quickly passes the potential minimum and then climbs up toward the starting point F_1. It takes a long time for the object to reach F_1, where the object stays. This represents a solitary trajectory to be shown in the following.

4.5.1. Analytical Periodic Solutions

As illustrated in Fig. 3, the solution of (38b) for $C_1 \neq 0$ is periodic. The analytical solutions of (38a) are also found in a few special cases as illustrated in the following.

(1) For $\varpi > 0$. Let $\eta_1 = (2\varpi)^{1/2}\xi$ and $F(\xi) = F_1 y(\eta_1)$, (38a) is normalized to

$$y'' + (1 - V_l/\varpi)\, y + \left(AF_1^2/\varpi\right) y^3 = 0 \tag{39a}$$

where $y'' = d^2y/d\eta_1^2$. For $V_l = AF_1^2$, i.e., $F_1^2 = -(\Delta\omega^2 C_s/\omega_{pi}^2 v_{te}^2)$, the solution of (39a) is a Jacobi elliptic function $cn(\eta_1, \gamma_1)$, where $\gamma_1 = (V_l/2\varpi)^{1/2}$. Because $F_1^2 > 0$, it requires that $\Delta\omega^2 < 0$; namely, the nonlinear periodic solution exists in the region above the matching height.

(2) For $\varpi < 0$ and $\Delta\omega^2 > 0$. Let $\eta_2 = (2|V_l|)^{1/2}\xi$ and $F(\xi) = F_2 y(\eta_2)$, (38a) is normalized to

$$y'' + (1 - |\varpi|/|V_l|)y + \left(AF_2^2/|V_l|\right) y^3 = 0 \tag{39b}$$

where $y'' = d^2y/d\eta_2^2$. For $|\varpi| = AF_2^2$, i.e., $F_2^2 = (6|\varpi|k_1^2 C_s^2/\omega_{pi}^{2)}$, the solution of (39b) is a Jacobi elliptic function $cn(\eta_2, \gamma_2)$, where $\gamma_2 = (|\varpi/2V_l|)^{1/2}$.

(3) For $\varpi = 0$ and $\Delta\omega^2 < 0$. Let $\eta_3 = (V_l)^{1/2}\xi$ and $F(\xi) = F_3 y(\eta_3)$, (38a) is normalized to

$$y'' - 2y + \left(2AF_3^2/V_l\right) y^3 = 0 \tag{39c}$$

where $y'' = d^2y/d\eta_3^2$. For $V_l = AF_3^2$, i.e., $F_3^2 = -(\Delta\omega^2 C_s/\omega_{pi}^2 v_{te}^2)$, the solution of (39c) is a Jacobi elliptic function $dn(\eta_3, 0)$.

4.5.2. Solitary Solution

Consider a localized solution of (38a), it requires that $F = 0 = F'$ as $|\xi| \to \infty$. Thus, $C_1 = 0$, and (38b) is re-expressed to be

$$F'^2 - \alpha F^2 + AF^4 = 0 \tag{40}$$

where $\alpha = -\Lambda = 2(V_l - \varpi)$. A solitary solution of (40) is given by

$$F(\xi) = (\alpha/A)^{1/2}\mathrm{sech}\sqrt{\alpha}\xi \tag{41}$$

subject to $\alpha > 0$; it requires that $\Delta\omega^2 < -6\varpi k_1^2 v_{te}^2$. Again, it exists in the region above the matching height as well as higher than that of the nonlinear periodic solution.

Soliton is the result of the balance between the dispersion effect (represented by the second term on the LHS of (37) and the nonlinearity (represented by the third term on the LHS of (37) of the medium. The nonlinearity of the medium focuses the wave to overcome the wave dispersion in the propagation, thus a shape-preserved solitary wave can exist. It is noted that the solitary solution exists only under the condition $\varpi < V_l$, i.e., the wave energy is less than the linear potential energy. Because soliton is a localized entity, several solitons can appear simultaneously and interact each other in the transient period [20].

It is shown that plasma can support Langmuir soliton, but Langmuir soliton is not a necessity of the plasma nonlinearity; the solution form of the nonlinear Schrodinger equation, either a periodic

function or a solitary function, depends on the initial/boundary conditions of the source wave function. In heating experiments, heating wave covers a large cross section area (a few tens of km in diameter). Therefore, under the normal condition, it is not likely to excite localized Langmuir waves as the source waves to evolve nonlinearly into Langmuir solitons.

ACKNOWLEDGMENT

I am grateful to M. C. Lee, MIT, to Paul Kossey, Air Force Research Laboratory at Hanscom Air Force Base, to Lee Snyder, NorthWest Research Associates, Inc., and to Edward Kennedy, Naval Research Laboratory, for helpful discussions.

This work was supported by the High Frequency Active Auroral Research Program (HAARP), AFRL at Hanscom AFB, MA, and by the Office of Naval Research, Grant No. ONR-N00014-10-1-0856. Part of the financial support was arranged through NorthWest Research Associates, Inc. under Air Force Research Laboratory contract FA8718-08-C-0049.

REFERENCES

1. Kuo, S. P., "Basis of ionospheric modification by high-frequency waves," *Progress in Electromagnetics Research*, Vol. 73, 277–296, 2007.
2. Budden, K. G., *Radio Waves in the Ionosphere*, Cambridge University Press, Cambridge, 1961.
3. Fejer, J. A., "Ionospheric modification and parametric instabilities," *Rev. Geophys.*, Vol. 17, 135–153, 1979.
4. Perkins, F. W., C. Oberman, and E. J. Valeo, "Parametric instabilities and ionospheric modification," *J. Geophys. Res.*, Vol. 79, 1478–1496, 1974.
5. Kuo, S. P., "Oscillating two stream instability in ionospheric heating experiments," *Phys. Plasmas*, Vol. 9, 1456–1459, 2002.
6. Kuo, S. P., B. R. Cheo, and M. C. Lee, "The role of parametric decay instabilities in generating ionospheric irregularities," *J. Geophys. Res.*, Vol. 88, 417–423, 1983.
7. Braginskii, S. I., *Transport Process in a Plasma, Reviews of Plasma Physics*, Vol. 1, 205, M. A. Loentovid, Ed., Consultant's Bureau, New York, 1965.
8. Kuo, S. P., "The role of nonlinear beating currents on parametric instabilities in magnetoplasmas," *Phys. Plasmas*, Vol. 3, No. 11, 3957–3965, 1996.
9. Kuo, S. P., "Cascade of the parametric decay instability in ionospheric heating experiments," *J. Geophys. Res.*, Vol. 106, 5593–5597, 2001.
10. Kuo, S. P. and M. C. Lee, "Cascade spectrum of HFPLs generated in HF heating experiments," *J. Geophys. Res.*, Vol. 110, A01309, 2005, Doi: 10.1029/2004JA010674.
11. Kosch, M., T. Pedersen, J. Hughes, R. Marshall, E. Gerken, A. Senior, D. Sentman, M. McCarrick, and F. Djuth, "Artificial optical emissions at HAARP for pump frequencies near the third and second electron gyro-harmonic," *Ann. Geophys.*, Vol. 23, 1585–1592, 2005.
12. Kuo, S. P. and G. Schmidt, "Filamentation instability in magneto plasmas," *Phys. Fluids*, Vol. 26, 2529–2536, 1983.
13. Minkoff, J., "Radio frequency scattering from a heated ionospheric, Volume: 3, Cross section calculations," *Radio Sci.*, Vol. 9, 997–1004, 1974.
14. Frey, A., P. Stubbe, and H. Kopka, "First experimental evidence of HF produced electron density irregularities in the polar ionosphere; diagnosed by UHF radio star scintillations," *Geophys. Res. Lett.*, Vol. 11, 523–526, 1984.
15. Kuo, S. P., W. E. Cheng, J. A. Cohen, R. Pradipta, M. C. Lee, S. C. Kuo, and A. Snyder, "Simultaneous generation of large-scale density irregularities and geomagnetic pulsations via filamentation instability," *Geophys. Res. Lett.*, Vol. 36, L09107, 2009, Doi: 10.1029/2009GL037942.
16. Stenflo, L. and P. K. Shukla, "Filamentation instability of electron and ion cyclotron waves in the ionosphere," *J. Geophys. Res.*, Vol. 93, 4115–4117, 1988.

17. Lee, M. C., R. J. Riddolls, W. J. Burke, S. P. Kuo, and E. M. C. Klien, "Generation of large sheet-like ionospheric plasma irregularities at Arecibo," *Geophys. Res. Lett.*, Vol. 25, 3067–3070, 1998.
18. Schmidt, G., *Physics of High Temperature Plasmas*, 2nd Edition, Chapter 9, 304–318, Academic Press, 1979.
19. Kuo, S. P., "On the nonlinear plasma waves in the high-frequency (HF) wave heating of the ionosphere," *IEEE Trans. Plasma Sci.*, Vol. 42, No. 4, 1000–1005, 2014; Doi: 10.1109/TPS.2014.2306834.
20. Konar, S. and A. Biswas, "Soliton-soliton interaction with power law nonlinearity," *Progress In Electromagnetics Research*, Vol. 54, 95–108, 2005.